Theoretical and experimental study on broadband terahertz atmospheric transmission characteristics*

Shi-Bei Guo(郭拾贝)[1,2], Kai Zhong(钟凯)[1,2,†], Mao-Rong Wang(王茂榕)[1,2], Chu Liu(刘楚)[1,2], Yong Xiao(肖勇)[3], Wen-Peng Wang(王文鹏)[3], De-Gang Xu(徐德刚)[1,2], and Jian-Quan Yao(姚建铨)[1,2]

[1] *Institute of Laser and Opto-electronics, College of Precision Instrument and Opto-electronics Engineering, Tianjin University, Tianjin* 300072, *China*

[2] *Key Laboratory of Opto-electronics Information Technology (Ministry of Education), Tianjin University , Tianjin* 300072, *China*

[3] *National Key Laboratory of Science and Technology on Millimeter-wave Remote Sensing, Beijing* 100039, *China*

(Received 31 July 2016; revised manuscript received 17 September 2016; published online 30 November 2016)

Broadband terahertz (THz) atmospheric transmission characteristics from 0 to 8 THz are theoretically simulated based on a standard Van Vleck–Weisskopf line shape, considering 1696 water absorption lines and 298 oxygen absorption lines. The influences of humidity, temperature, and pressure on the THz atmospheric absorption are analyzed and experimentally verified with a Fourier transform infrared spectrometer (FTIR) system, showing good consistency. The investigation and evaluation on high-frequency atmospheric windows are good supplements to existing data in the low-frequency range and lay the foundation for aircraft-based high-altitude applications of THz communication and radar.

Keywords: terahertz atmospheric propagation, line absorption, continuum absorption

PACS: 95.85.Gn, 92.60.Ta, 42.68.Ay **DOI:** 10.1088/1674-1056/26/1/019501

1. Introduction

The terahertz (THz) spectral range (30–3000 μm or 0.1–10 THz), which falls between microwave and infrared, has received a great deal of attention due to its importance in spectroscopy, imaging, communication, remote sensing, radar, and so on. Despite the remarkable achievement made on THz sources, detectors, functional devices, etc., there are still some existing obstacles before widely practical applications are spread out, especially in long-range systems because of the prominent absorption caused by intense rotational transitions of the atmospheric molecules (mainly water) in the ambient atmosphere.[1,2] As water vapor pervades the entire atmosphere, to characterize the absorption by water in the entire THz range, in other words, to find atmospheric windows where THz waves are not wholly absorbed by water, is the primary task before designing a THz system. These atmospheric windows are located between strong resonant absorption lines defined by their center, strength, and broadening. Sometimes, it is difficult to explain the discrepancy between theoretical and experimental results. As a result, the empirically defined continuum absorption, which has not been clearly interpreted yet, was introduced.[3–5]

Since worldwide attention was paid to the cutting-edge THz technology in the last two decades, a great deal of work was performed to understand the absorption characteristics of water vapor in the THz range, including line absorption and continuum absorption. Even though existing theoretical calculations can predict atmospheric windows with the open HITRAN data and codes on the dependence of the THz absorption,[6–10] direct precise experimental methods are still necessary, which provide the most reliable results. Plenty of work has been done on measuring the atmospheric absorption characteristics based on terahertz time-domain systems (TDS) and infrared Fourier transform spectrometers (FTIR).[3,11–16] However, most of the previous theoretical and experimental work concentrated on constant normal pressure and temperature (*NPT*) only, which is insufficient to depict the accurate width of the atmospheric windows as they should be significantly changed at high-altitude conditions or in the upper atmosphere. Moreover, the lack of research on atmospheric propagation characteristics in the high-frequency range (above 3 THz) limits the applications of some superior THz sources such as quantum cascade lasers (QCL).

In this paper, we demonstrated the calculation of THz propagation covering a wide band from 0 to 8 THz with HITRAN data, considering the dependence of humidity, pressure, and temperature. For verification, a laboratory experimental system was built based on FTIR in the 0.5–7.5 THz range and measurements were performed at different humidities and pressures. It is believed to be the first report to predict new high-frequency atmospheric windows. The conclusions are of great importance for high-resolution radar and high-capacity wireless communication applications among airplanes, aerospace planes, reentry capsules, and satellites

*Project supported by the National Basic Research Program of China (Grant Nos. 2014CB339802 and 2015CB755403), the National Natural Science Foundation of China (Grant Nos. 61675146, 61275102, and 61271066), and the Science and Technology Support Program of Tianjin, China (Grant No. 14ZCZDGX00030).

†Corresponding author. E-mail: zhongkai1984@gmail.com

© 2017 Chinese Physical Society and IOP Publishing Ltd

from the upper atmospheric to near-Earth orbit.

2. Theoretical calculation

The absorption lines describe the probability of absorption and emission originating from energy-level transitions of certain atmospheric molecules. Although transitions generate definite single discrete lines, in reality they are broadened under the influence of external conditions into absorption bands which have special shapes with centers at the transition frequencies and decreased wings. Theoretically, the atmospheric absorption coefficient κ at a certain frequency is a combined effect of different transitions of one or multi molecule species, and is expressed as [17]

$$\kappa = \sum_i \kappa_i = \sum_i S_i F(\nu - \nu_i), \tag{1}$$

where κ_i is the absorption coefficient of line i at frequency ν, S_i is the corresponding transition strength, ν_i is the central frequency of line i, and $F(\nu - \nu_i)$ is the normalized spectral line shape function. All the parameters mentioned above depend on the molecule species, temperature, and pressure. If the position and line shape of all absorbing atmospheric molecules are identified, the precise calculation of absorption at certain frequencies can be performed.

The transition strength per unit volume of a single molecule between two rotational states is given by[17]

$$S_{i,\mathrm{M}} = \frac{A_i}{8\pi c \nu_i^2} \frac{g' \mathrm{e}^{-hcE''/kT}(1 - \mathrm{e}^{-hc\nu_i/kT})}{Q(T)}, \tag{2}$$

where A_i is the Einstein spontaneous emission coefficient, g' is the upper-level statistical distribution weight, E'' is the lower-level energy, $Q(T)$ is the total internal partition function, h is the Planck constant, k is the Boltzmann constant, and c is the velocity of light. Then the transition strength of line i can be obtained with $S_i = NS_{i,\mathrm{M}}$, in which $N = p/kT$ is the volume density of the corresponding molecule and p is its partial pressure.

The Van Vleck–Weisskopf line shape function is given as[18]

$$F_{\mathrm{VVW}}(\nu - \nu_i) = \frac{\nu \Delta\nu}{\pi \nu_i} \left(\frac{1}{(\Delta\nu)^2 + (\nu - \nu_i)^2} + \frac{1}{(\Delta\nu)^2 + (\nu + \nu_i)^2} \right), \tag{3}$$

where $\Delta\nu$ is the half width of line i calculated by the following equation:

$$\Delta\nu = \gamma_{\mathrm{air}}(P - P_{\mathrm{s}}) + \gamma_{\mathrm{self}} P_{\mathrm{s}}. \tag{4}$$

Here P is the total pressure, P_{s} is the partial pressure of the related species, and γ_{air} and γ_{self} are the environment-broadened half width and the self-broadened half width, respectively.

All absorption lines of the 47 atmospheric molecules and their isotopes at different densities, temperatures, and pressures can be calculated with the theories mentioned above based on the data given by HITRAN.[13] It can be concluded that only water vapor and oxygen bring obvious absorption. The results at 50% relative humidity (RH), normal temperature, and ambient pressure (*NPT*, 296 K and 101.3 kPa) are shown in Fig. 1, where 1696 and 298 absorption lines for water and oxygen, respectively, are considered in the range of 0–8 THz. There are 56 absorption peaks induced by oxygen and much more by water. Overall, the water absorption increases with the increase of the frequency, while the oxygen absorption goes in the opposite direction. Water dominates in atmospheric absorption and should be mostly concerned above 120 GHz.

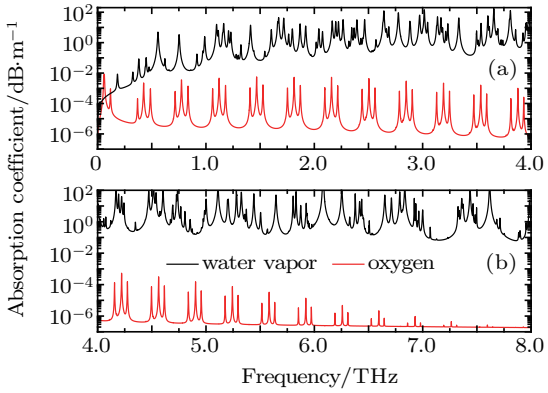


Fig. 1. (color online) Water vapor and oxygen absorption at *NPT* and 50% RH in the range of 0–8 THz.

Atmospheric line absorptions in the range of 0–8 THz at different humidities, temperatures, and pressures are shown in Figs. 2(a)–2(c), where both oxygen and water line absorptions are considered.[17] Apparently, most of the low-loss (< 100 dB/km at *NPT* and 50% RH) atmospheric windows are located in the low-frequency range, e.g., 0.087 THz, 0.128 THz, 0.21 THz, 0.34 THz, 0.41 THz, 0.67 THz, 0.85 THz, and 1.50 THz. The absorption coefficient increases with the increase of humidity, temperature, and pressure. Take the 1.5-THz window for example. The absorption coefficient increases by 4, 47, and 87 times when the relative humidity, temperature, and pressure are increased from 20% to 80%, −30 °C to 30 °C, and 10 kPa to 110 kPa, respectively. The losses of high-frequency windows like 1.98 THz, 2.52 THz, 3.44 THz, and 5.73 THz are higher than 100 dB/km at *NPT* and 50% RH, which limit their near-ground long-range applications. At high altitude or even the upper atmospheric layer, however, the loss obviously decreases with lower water concentration and pressure, thus there is no barrier for radar and communication. We can also conclude that the absorption line width becomes narrower with the decline of the absorption coefficient, which is good news for high-altitude applications with broader atmospheric windows.

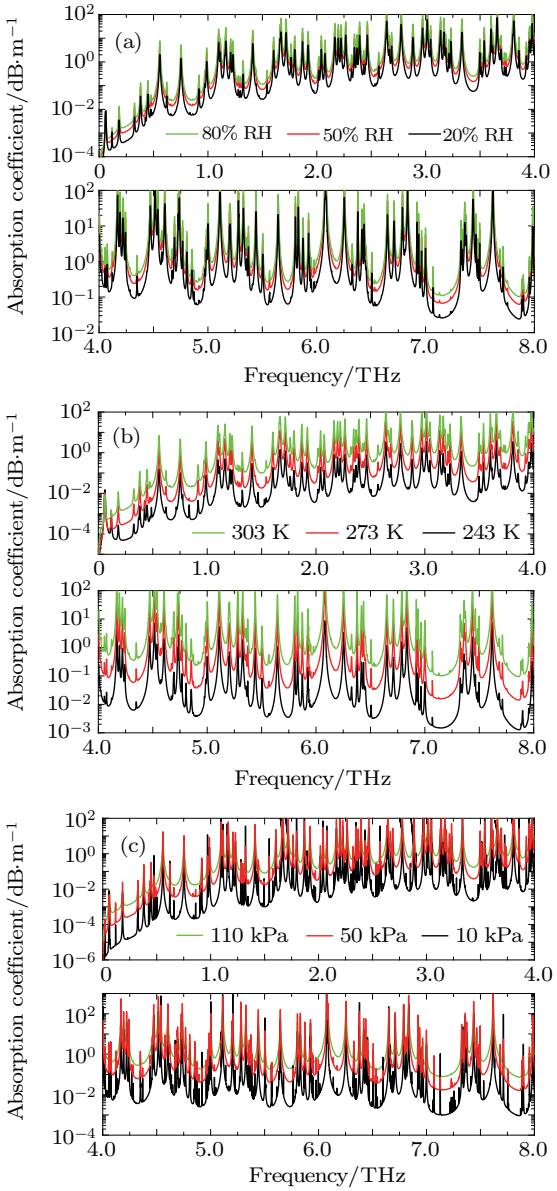


Fig. 2. (color online) Atmospheric line absorptions in the range of 0–8 THz at different humidities, temperatures, and pressures. Calculations are performed at (a) *NTP*, (b) 101.3 kPa and 50% RH, (c) 296 K and 50% RH.

3. Experimental setup and results

In order to verify the accuracy of theoretical simulations, an experimental system was built based on an FTIR (SCIENCETECH SPS-300) equipped with a chamber serving as the gas cell, which enabled direct measurement on THz atmospheric propagation characteristics in the laboratory, as shown in Fig. 3. The internal light source of the FTIR was a mercury arc lamp with the maximum power of 75 W, covering a wide band from mid- to far-infrared. A fixed roof mirror, a moveable roof mirror, as well as a mylar beam splitter composed the Michelson interferometer. The moveable mirror was mounted on a 300-mm-long stage, yielding a resolution as high as 0.02 cm^{-1}. The chamber, which was connected to the FTIR by a long aluminum pipe to increase the path length, had a humidity sensor and a vacuum gauge. All the reflecting mirrors were coated with gold for high-reflection. A liquid-helium cooled (4.2 K) silicon bolometer was used as the detector with a white polyethylene (PE) adaptor to the chamber. The total effective absorption path length was 2.3 m. The whole system could maintain a vacuum up to 10^{-3} Torr with a mechanical vacuum pump.

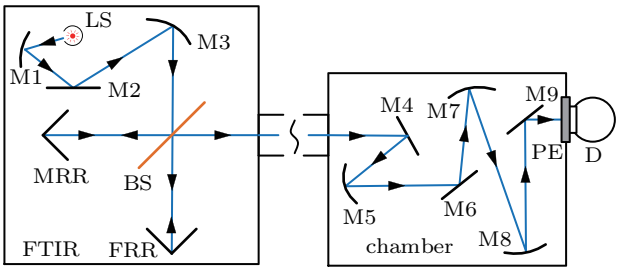


Fig. 3. (color online) Experimental system for in-laboratory measurement of atmospheric propagation characteristics. LS: light source, M1, M3, M5, M7, and M8: spherical reflectors, M2, M4, M6, and M9: plane reflectors, MRR: moveable roof reflector, FRR: fixed roof reflector, BS: beam splitter, D: detector.

Although ideally the FTIR had a spectral range from 8 cm^{-1} (0.24 THz) to above 1000 cm^{-1} (30 THz), the actual available range was from 0.5 THz to 7.5 THz limited by the cutoff frequency of the beam splitter and the internal filter of the detector. The weak intensity of the mercury lamp at the low frequency end also restricted the corresponding signal-to-noise ratio (SNR). The resolution was set to be 0.4 cm^{-1} considering a reasonable scanning time and the internal memory of the computer. Figure 4 shows the typical background interferogram at the pressure of 50 Pa as well as the spectrum obtained by Fourier transform. The SNR of the interferogram was over 2000 after averaging 10 times. Distinct water absorption lines at the high-frequency range could still be seen due to the high absorption coefficient of residual gas although pumped to low pressure. It should be noted that the prominent dip at 2.25 THz was caused by absorption of the PE adaptor, which would not affect data processing as it was considered in the reference (background). Through comparison between spectra of the actual atmosphere and the background, THz transmission T in the actual atmosphere was obtained and the absorption coefficient α was calculated from the Beer–Lambert law $T = \mathrm{e}^{-\alpha L}$, where L is the effective absorption path length.

The required pressure and humidity were realized by vacuum pumping and injection of water vapor from a humidifier through the air inlet valve mounted on the chamber. In some cases, dry air was needed to balance the relation between pressure and humidity. Sufficient diffusion time for water moleculars also ensured an identical humidity distribution in the whole system. For identical humidity at different pressures, the THz transmission was measured from 0.5–7.5 THz, as shown in Fig. 5. Although several absorption lines below 0.8 THz could be distinguished, such as 0.56 THz and

0.75 THz, the absolute value was obviously inaccurate because of the low SNR in this range and abnormal transmissions above 100%. Undoubtedly absorption increased with pressure and narrower absorption lines were observed at lower pressure. At the same pressure and temperature (*NPT*), THz propagation characteristics at different relative humidities are shown in Fig. 6. All of the theoretical predictions accorded with the experimental results.

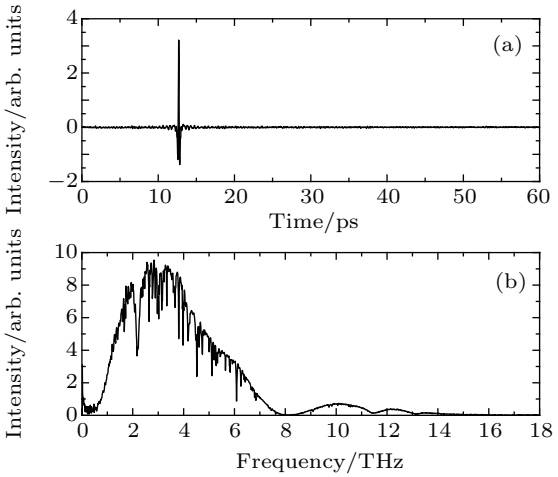


Fig. 4. (a) Interferogram and (b) spectrum of the background.

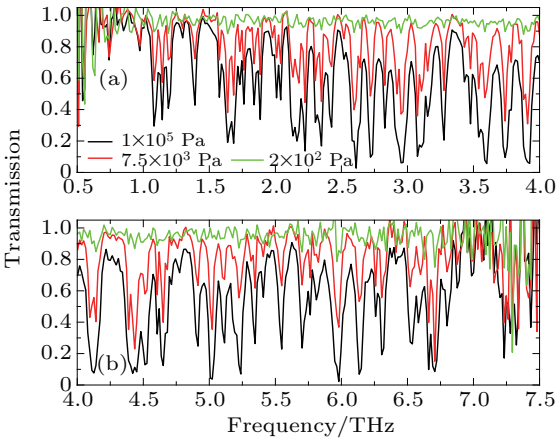


Fig. 5. (color online) THz transmission of 0.5–7.5 THz at different pressures.

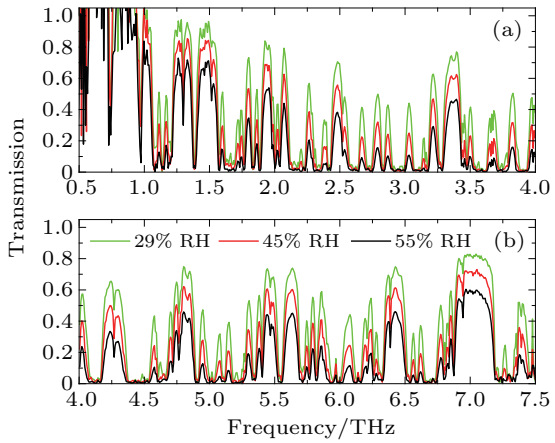


Fig. 6. (color online) THz transmission at different relative humidities.

4. Analysis and discussion

The experimental measurements at 45% RH and *NPT* were compared with the theoretical results for quantitative verification. It was found that if we merely considered line absorptions in the calculation, there were apparent deviations (the experimental absorptions were higher) especially at high-transmission windows, which should be attributed to continuum absorption. Figure 7 shows the comparison while the continuum absorption was taken into account using the MT-CKD model,[19] which is valid all over the THz range. The absorption coefficient used for calculating transmission in Fig. 7 was the summation of the continuum absorption coefficient and the line absorption coefficient. Obviously, extremely good consistency was obtained during the whole measurement range, proving the accuracy of both theoretical and experimental methods.

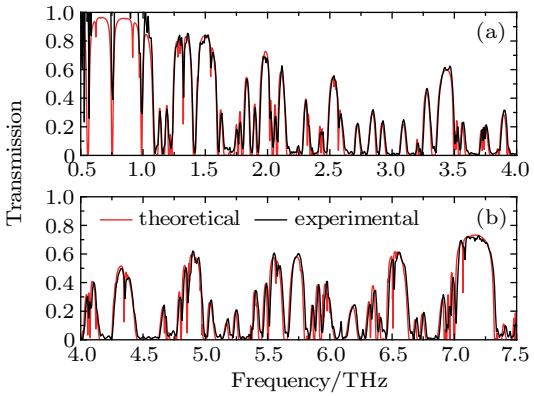


Fig. 7. (color online) Comparison of experimental and theoretical transmission at 45% RH and *NPT*.

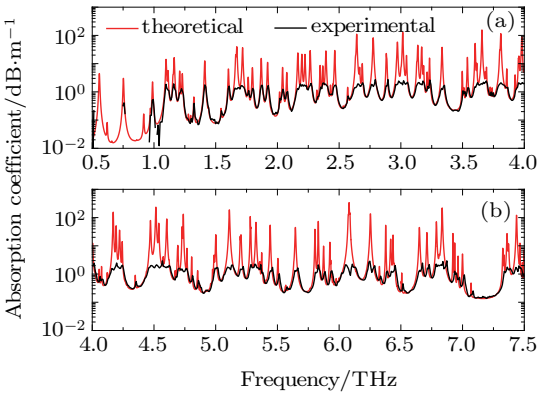


Fig. 8. (color online) Comparison of experimental and theoretical absorption coefficients at 45% RH and *NPT*.

Calculated based on the actual experimental path length and the Beer–Lambert law, the absorption coefficients at 45% RH and *NPT* are demonstrated in Fig. 8. Comparing with the theoretical results, the variation tendency was almost the same. However, there was a large discrepancy between their absolute values at the absorption peaks owing to two main

reasons. Firstly, the limited SNR of the FTIR was not high enough to distinguish a very weak signal, then when encountering serious absorption, the absolute value of transmission (output voltage of the detector) which was the basis for calculating the absorption coefficient, was not accurate enough. A slight error in transmission (e.g., 0.1% and 0.2%) would cause a huge difference in the absorption coefficient. Secondly, the resolution of the FTIR was too low to distinguish some narrow absorption peaks as the actual spectrum resolution in the measurement was much lower than that in the calculation. This phenomenon should be even more significant at low-pressure conditions when the absorption peaks were even narrower. Nevertheless, the experimental data for high transmission are reliable, sufficient for characterizing atmospheric transmission windows which are useful in designing THz systems.

The main atmospheric windows from 1 THz to 7.5 THz based on the theoretical results of line absorption and continuum absorption are summarized and listed in Table 1. Three different altitudes (0 km, 10 km, and 30 km) covering from the ground to the stratosphere layer were selected for comparison. All the data were obtained with standard 45% RH atmosphere conditions at sea level. Bandwidths were defined by the half maximum transmissions (3-dB) of the corresponding windows over the 1-km range.

Table 1. Main transmission windows from 1 THz to 7.5 THz.

Central frequency/THz	Absorption coefficient/dB·m^{-1}			Bandwidth/GHz		
	0 km	10 km	30 km	0 km	10 km	30 km*
1.024	0.073	1.15×10^{-4}	1.97×10^{-12}	5	66	–
1.342	0.082	9.92×10^{-5}	1.72×10^{-12}	4	73	–
1.502	0.078	1.06×10^{-4}	2.36×10^{-12}	7	57	–
1.984	0.139	1.80×10^{-4}	2.96×10^{-12}	8	80	–
2.524	0.263	3.25×10^{-4}	5.96×10^{-12}	4	44	–
3.437	0.224	2.58×10^{-4}	4.43×10^{-12}	14	133	–
4.902	0.224	2.65×10^{-4}	6.08×10^{-12}	5	61	–
5.548	0.240	2.77×10^{-4}	4.56×10^{-12}	5	112	–
5.734	0.239	2.61×10^{-4}	4.31×10^{-12}	8	121	–
7.163	0.136	1.52×10^{-4}	2.52×10^{-12}	40	252	–

* Bandwidths were not limited by transmission windows.

From Table 1, it can be seen that the absorption coefficients increase with frequency until 3 THz and begin to decrease due to the combined impacts of line absorption and continuum absorption.[8] As the meteorological conditions are not uniform, there are slight differences among the variation trends at different altitudes. Although few high-frequency atmospheric windows at *NPT* are available for practical long-range applications, THz absorption in most of the windows at high altitude is negligible and good enough for radar and communication. At the stratosphere and mesosphere layers where activities of airplanes, high altitude balloons, and aerospace planes exist, the water concentration, temperature, and pressure are even lower, thus there is no barrier for long-range applications. THz windows above plasma resonant frequency also provide ideal approaches to solve the black-out problem for a reentry capsule through communication with relay satellites. Moreover, higher frequency is a known-to-all advantage to enhance communication capacity and radar resolution. The high loss in the lower atmosphere layer also avoids ground-based monitoring as well, ensuring communication security.

Figure 9 depicts the feasibility of long-range applications at different altitudes with 4 typical windows at 1.502 THz, 3.438 THz, 5.734 THz, and 7.149 THz by evaluating their transmissions. At the altitude above 6.44 km, 10-km communication between airplanes is possible using the 7.15-THz window with absorption loss less than 30 dB. Above 9.65 km, 100-km long-range radar is practical. THz applications for near-space aerocrafts are almost unrestricted above 20 km.

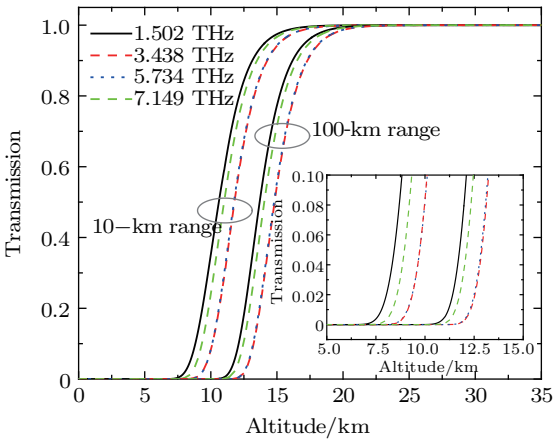


Fig. 9. (color online) Long-range THz transmission at different altitudes at high-frequency windows. The inset is the partial amplification of the low transmission part from 5 THz to 15 THz.

5. Conclusion

Wide-band THz atmospheric propagation characteristics were investigated both theoretically and experimentally. Con-

sidering the influence of water concentration, temperature, and pressure, we calculated the absorption coefficients from 0 to 8 THz, which were verified by an FTIR-based measurement system with good consistency in their coincident applicable range. Based on our results, the high-frequency atmospheric windows were evaluated and the feasibility for long-range applications was estimated. The data obtained proved the advantage of THz applications for high-altitude aircraft and were of great importance for designing THz systems.

References

[1] Siegel P H 2002 *IEEE T. Microw. Theory* **50** 910

[2] Hosako I, Sekine N, Patrashin M, Saito S, Fukunaga K, Kasai Y, Baron P, Seta T, Mendrok J, Ochiai S and Yasuda H 2007 *Proc. IEEE* **95** 1611

[3] Slocum D M, Slingerland E J, Giles R H and Goyette T M 2013 *J. Quant. Spectrosc. Ra.* **127** 49

[4] Yang Y, Mandehgar M and Grischkowsky D 2014 *Opt. Express* **22** 4388

[5] Shine K P, Ptashnik I V and Rädel G 2012 *Surv. Geophys.* **33** 535

[6] Liebe H J 1989 *Int. J. Infrared Milli.* **10** 631

[7] Pardo J R, Cernicharo J and Serabyn E 2001 *IEEE T. Antenn. Propag.* **49** 1683

[8] Urban J, Baron P, Lautié, Schneider N, Dassas K, Ricaud P and De La Noë J 2004 *J. Quant. Spectrosc. Ra.* **83** 529

[9] Clough S A, Shephard M W, Mlawer E J, Delamere J S, Iacono M J, Cady-Pereira K, Boukavara S and Brown P D 2005 *J. Quant. Spectrosc. Ra.* **91** 233

[10] Rothman L S, Rinsland C P, Goldman, et al. 1998 *J. Quant. Spectrosc. Ra.* **60** 665

[11] Seta T, Mendrok J and Kasai Y 2008 *URSI Chicago General Assembly* 14

[12] Jiang Y, Liang M, Jin B B, Kang L, Xu W W, Chen J and Wu P H 2012 *Chin. Sci. Bull.* **57** 573

[13] Yang Y, Mandehgar M and Grischkowsky 2012 *Opt. Express* **20** 26208

[14] Moon E B, Jeon T I and Grischkowsky D R 2015 *IEEE Trans. Terahertz Sci. Technol.* **5** 742

[15] Wang Y W, Dong Z W, Li H Y, Zhou X, Deng H and Luo Z F 2015 *J. Infrared Millim. Waves* **34** 557 (in Chinese)

[16] Wang Y W, Dong Z W, Li H Y, Zhou X and Luo Z F 2016 *Acta Phys. Sin.* **65** 134101 (in Chinese)

[17] http://hitran.org/

[18] Van Vleck J H and Weisskopf V F 1945 *Rev. Mod. Phys.* **17** 227

[19] Mlawer E J, Payne V H, Moncet J L, Delamere J S, Alvarado M J and Tobin D C 2012 *Phil. Trans. R. Soc. A* **370** 2520